

Temporal Evolution of Plunge Pool Scour

Stefano Pagliara¹; Willi H. Hager, F.ASCE²; and Jens Unger³

Abstract: The temporal development of plunge pool scour was investigated using a novel experimental approach. Longitudinal profiles along the scour hole were recorded with an optical method to allow its definition at any time, from the initiation of scour to nearly the end-scour condition. The characteristics of the scour hole geometry were investigated, namely the maximum scour hole depth, the maximum ridge height, and their locations relative to the scour hole origin. It is demonstrated that the evolution is logarithmic, similar to that found for bridge pier and abutment scour. A distinction is further made between the developing and the developed scour hole phases. The main issue of the present research was to define the developed scour hole characteristics because the developing scour phase is influenced by turbulence features that may be difficult to assess. This work therefore allows for an appreciation of the temporal evolution of a scour process of engineering interest.

DOI: 10.1061/(ASCE)0733-9429(2008)134:11(1630)

CE Database subject headings: Hydraulic structures; Scour; Sediment; Spillways; Water flow; Pools.

Introduction

Plunge pool scour received significant attention in the past few years from a collaboration between Versuchsanstalt für Wasserbau, Hydrologie and Glaziologie (VAW), of ETH Zurich, and Università di Pisa, Italy (Canepa and Hager 2003; Pagliara et al. 2004, 2006, 2008). In the first paper, the applicability of the dimensionless Froude number was verified for the three phase flow composed of a water or an air-water mixture jet scouring a sediment surface and eventually entraining air, as was previously suggested by Rajaratnam and Berry (1977) and Rajaratnam (1980). The results pertained to relatively large jet Froude numbers compared to those considered by Anderson and Blaisdell (1982) and Bormann and Julien (1991). Dey and Barbhuiya (2005) developed a semiempirical model to compute the temporal variation of scour depth for short abutments. Pagliara et al. (2008) extended previous results to the three-dimensional (3D) scour hole arrangement including hydraulic and granulometric effects. They added to the effect of the relative scour hole width, both the static and the dynamic scour hole depths, the spatial scour hole extension, the scour hole and the suspended sediment volume under dynamic scour conditions, and the maximum ridge height, a feature previously studied by Chiew and Lim (1996). These relations considered conditions close to end scour, i.e., when a temporal scour advance is no longer discernable.

The question of how a plunge pool scour hole temporally develops is addressed in the present work through detailed addi-

tional experiments conducted at VAW. Using a novel experimental method, the main effects were investigated based on the previous test results. The results of the present work are presented such that they may be applied under well defined conditions and to also prototype scour holes made from granular mixtures if effects of viscosity are negligible.

Experiments

Experimental Procedure

The tests were conducted at the VAW scour channel previously described by Hager et al. (2002). Because only the temporal development of plunge pool scour was studied, the test program involved one nearly uniform sediment with a median diameter $d_{50}=0.00115$ m, $d_{90}=0.00135$ m, and a sediment nonuniformity parameter $\sigma=(d_{84}/d_{16})^{1/2}=1.15$. Black water jets were produced with a high-precision pump attached to a piping system that was mounted on an adjustable carriage over the test channel (Fig. 1). The jet diameters were $D_{\text{test}}=0.0217$ and 0.0350 m (± 0.0005 m), and the jet impact angles $\alpha=30$, 45 , and 60° ($\pm 0.2^\circ$) from the horizontal (Fig. 2).

At this test beginning, the sediment surface was horizontal within an accuracy of about d_{50} (Hager et al. 2002). Then, the tailwater level was set to within ± 1 mm. The pump was directly supplied from the test channel such that its water elevation remained constant during a test. The jet was deflected from the sediment bed until the test discharge Q was within $\pm 1\%$. The time was set to $t=0$ at the instant when the jet impacted the sediment bed. To allow for a close visualization of the scour hole, a half-model arrangement was applied. The jet was therefore issued within a distance of 2–3 mm parallel to the glass channel wall. The equivalent jet diameter $D=2^{1/2}\cdot D_{\text{test}}$ of the half model accounted for this setup, thereby requiring equal jet velocity as for the full model. Preliminary observations with jets issued at the channel axis to check the applicability of this method indicated that the boundary layer effect on the jet features along the glass wall was small (Unger and Hager 2007). The scour hole profile and the scour hole plan geometry were recorded for selected tests

¹Professor, Dipt. di Ingegneria Civile, Univ. di Pisa, Via Gabbia 22, I-56100 Pisa, Italy (corresponding author). E-mail: s.pagliara@ing.unipi.it

²Professor, VAW, ETH-Zurich, CH-8092 Zurich, Switzerland.

³Ph.D. Candidate, INROS LACKNER AG, 18119 Rostock, Germany; formerly, VAW, ETH-Zurich, CH-8092 Zurich, Switzerland.

Note. Discussion open until April 1, 2009. Separate discussions must be submitted for individual papers. The manuscript for this paper was submitted for review and possible publication on September 27, 2006; approved on March 11, 2008. This paper is part of the *Journal of Hydraulic Engineering*, Vol. 134, No. 11, November 1, 2008. ©ASCE, ISSN 0733-9429/2008/11-1630-1638/\$25.00.

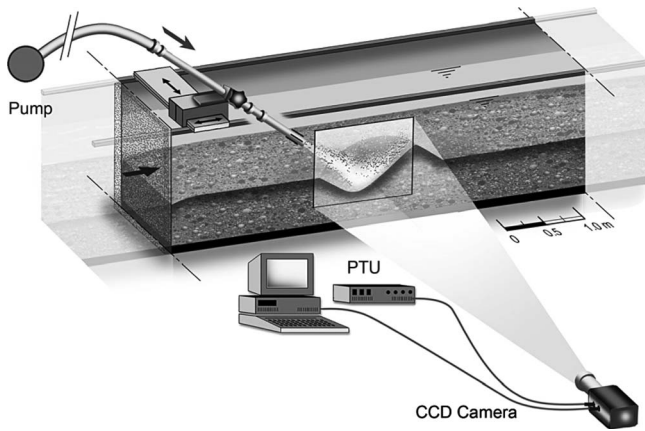


Fig. 1. Sketch of experimental setup

using a point gauge. A comparison with the half-model arrangement revealed negligibly small differences such that the latter approach was applied in the main test program.

The longitudinal scour hole profiles were recorded optically with a monochrome progressive scan charge coupled device (CCD) camera. The image acquisition was controlled with a programmable timing unit (PTU) as a master clock setup ensuring an accurate time control from the test start. In contrast to the previous pointwise recordings of the scour hole profile, a longitudinal scour hole profile could be recorded within one time instant. Fig. 1 shows a scheme of the setup used for the plunge pool scour research. It was important that neither air bubbles nor suspended sediment hindered the optical access to the flow field. These conditions were not always established due to sediment resuspension and air entrained by a jet. When the sediment surface was only partially visible at one instant, conditions improved shortly thereafter allowing for an accurate definition of the entire scour hole profile. In addition, postprocessing with a high-pass filter increased the image contrast.

Due to the logarithmic scour evolution, images were automatically captured at a rate of 1 Hz at the scour beginning, whereas the acquisition interval was later increased manually according to the test conditions. The CCD camera was calibrated using a 1.40 m × 0.70 m calibration plate with engraved crosses on a 40 mm grid positioned in the measuring plane. To increase the accuracy of the measuring system, all images were corrected to remove distortion (Unger 2006). The accuracy of the measured scour profiles was on the order of $\pm 2d_{50}$.

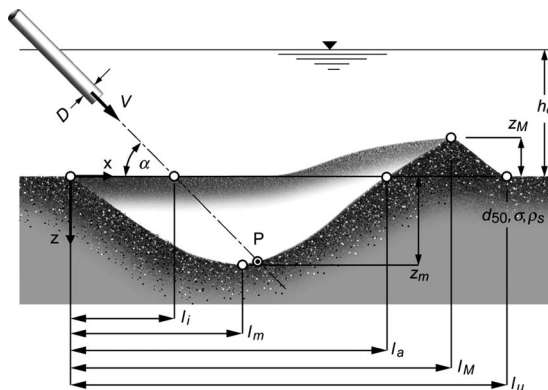


Fig. 2. Typical scour hole geometry, with notation

Experimental Program

The test program is summarized in Table 1. A total of 54 tests were conducted with test durations up to 1 day. Tests were carried out for both two-dimensional (2D) and 3D scour holes including submerged (S-jets) and unsubmerged (U-jets). For the latter, the jet impinged onto the water surface, whereas the tailwater elevation was higher than the pipe outlet for S-jets.

The test label in column 1 indicates the jet impact angle and the jet condition, e.g., T7A30S denotes for example Test 7 of Series A with a 30° jet impact angle for a submerged jet. Column 2 relates to the jet location in the scour channel with L indicating jets issued close to the glass wall (half-model arrangement), and C to tests in the channel center (full-model arrangement). Next, the jet impact angle α is specified, and column 4 gives the test duration. Column 5 states whether an S-jet or a U-jet was considered, the water discharge Q is given in column 6, column 7 states the relative tailwater submergence $T_{\text{test}} = h_o / D_{\text{test}}$ (Fig. 2), column 8 gives the equivalent jet diameter D , column 9 then the equivalent tailwater submergence with $D = 2^{1/2} D_{\text{test}}$ as explained, and column 10 relates to the tested jet diameter in the 3D hydraulic model. The densimetric particle Froude number based on the sediment size d_{90} is $F_{d90} = V / (g' d_{90})^{1/2}$ with $V = Q / (\pi D^2 / 4)$ as the average jet velocity, and $g' = [(\rho_s - \rho) / \rho] g$ as the reduced gravitational acceleration with ρ_s and ρ as the densities of sediment and water, respectively, as given in column 11.

Experimental Observations

Scour Hole Features

Figs. 3 and 4 show photographs of scour holes at various times t and $\alpha = 30$ and 60 , i.e., a small and a large jet impact angle. For $\alpha < 35^\circ$, the scour hole is essentially parabola shaped. Its origin is at location $x = 0$, the maximum (subscript m) scour depth z_m is at $x = l_m$, and its end at $x = l_a$ (Fig. 2). Downstream of the scour hole forms a sediment ridge of maximum (subscript M) height z_M above the original bed level at $x = l_M$ and the ridge ends at $x = l_u$. The final scour hole geometry close to the jet impact point P is cup shaped, whereas its angles close to the scour hole origin and the ridge are equal to the natural angle of repose in water ϕ of the sediment involved.

Fig. 3 shows images of Test T8A30S, i.e., $F_{d90} = 33.4$, $\alpha = 30^\circ$ for an S-jet issued from the upper left. From an initially horizontal sediment surface, surface turbulence is noted at $t = 1$ s due to jet impact. At $t = 4$ s, an almost symmetrical scour hole about the point of maximum scour depth forms, with sediment transport both in the longitudinal and the lateral directions. At $t = 8$ s, the scour hole shape becomes asymmetric, with a dominant longitudinal sediment transport. From $t = 12$ s, the sediment transport capacity is too small to transport all scoured material, resulting in a sediment deposition downstream of the flow recirculation above the scour hole. Accordingly, the sediment ridge is formed as an important scour feature. At $t = 51$ s, the upstream ridge portion is shaped, whereas the tailwater portion develops less fast because of limited sediment transport over the ridge. Note the comparatively large distances between the ridge maximum and the scour hole origin for $t = 51$ and 86 s as compared to smaller time, and the significant scour depth increase within this period. The *developing* scour phase is by now completed.

During the *developed* scour phase, the scour hole origin hardly changes until the test end, at $t = 3,400$ s, because its slope remains

Table 1. Experimental Test Program

Test	Jet position ^a	α (°)	Test duration (s)	Jet type (S/U)	Q (L/s)	$T_{\text{test}}=h_o/D_{\text{test}}$ (-)	D (m)	$T=h_o/D$ (-)	D_{test} (m)	F_{d90} (-)
T45A30S	3DL	30	68,820	S	0.8	18.3	0.03069	12.9	0.0217	14.8
T6A30S	3DL	30	7,000	S	1.2	18.3	0.03069	12.9	0.0217	22.3
T7A30S	3DL	30	6,100	S	1.5	18.3	0.03069	12.9	0.0217	27.8
T8A30S	3DL	30	3,600	S	1.8	18.3	0.03069	12.9	0.0217	33.4
T9A30S	3DL	30	2,000	S	2.1	18.3	0.03069	12.9	0.0217	39.0
T11A30U	3DL	30	4,000	U	2.1	16.8	0.03069	11.9	0.0217	39.0
T12A30U	3DL	30	5,000	U	1.8	16.8	0.03069	11.9	0.0217	33.4
T13A30U	3DL	30	7,000	U	1.5	16.8	0.03069	11.9	0.0217	27.8
T14A30U	3DL	30	1,800	U	2.4	16.8	0.03069	11.9	0.0217	44.5
T17A30U	3DL	30	52,000	U	1.2	16.8	0.03069	11.9	0.0217	22.3
T18A45S	3DL	45	7,000	S	0.7	12.4	0.03069	8.7	0.0217	13.0
T19A45S	3DL	45	7,000	S	1	12.4	0.03069	8.7	0.0217	18.6
T20A45S	3DL	45	5,000	S	1.7	12.4	0.03069	8.7	0.0217	31.5
T21A45S	3DL	45	3,000	S	2.5	12.4	0.03069	8.7	0.0217	46.4
T22A45U	3DL	45	53,000	U	1.5	10.1	0.03069	7.2	0.0217	27.8
T23A45U	3DL	45	10,000	U	0.9	10.1	0.03069	7.2	0.0217	16.7
T27A60S	3DL	60	4,000	S	1.6	9.9	0.03069	7.0	0.0217	29.7
T28A60S	3DL	60	50,000	S	1.2	9.9	0.03069	7.0	0.0217	22.3
T29A60S	3DL	60	6,000	S	2.2	9.7	0.03069	6.8	0.0217	40.8
T30A60U	3DL	60	4,000	U	1	7.2	0.03069	5.1	0.0217	18.6
T31A60U	3DL	60	7,000	U	1.5	7.2	0.03069	5.1	0.0217	27.8
T32A60U	3DL	60	4,000	U	2.2	7.2	0.03069	5.1	0.0217	40.8
T33A30U	3DL	30	7,000	U	3	9.4	0.04950	6.7	0.035	21.4
T34A30U	3DL	30	4,000	U	4.2	10.1	0.04950	7.2	0.035	30.0
T35A30U	3DL	30	40,000	U	2	10.9	0.04950	7.7	0.035	14.3
T36A30S	3DL	30	2,000	S	3.2	12.4	0.04950	8.8	0.035	22.8
T37A30S	3DL	30	600	S	4.5	12.4	0.04950	8.8	0.035	32.1
T38A30S	3DL	30	7,000	S	2	12.4	0.04950	8.8	0.035	14.3
T39A45S	3DL	45	3,000	S	4	9.0	0.04950	6.4	0.035	28.5
T40A45S	3DL	45	3,600	S	5.5	9.0	0.04950	6.4	0.035	39.2
T41A45S	3DL	45	7,000	S	2	9.0	0.04950	6.4	0.035	14.3
T42A45U	3DL	45	53,000	U	2	8.3	0.04950	5.9	0.035	14.3
T43A45U	3DL	45	3,600	U	5	8.3	0.04950	5.9	0.035	35.7
T44A45U	3DL	45	7,000	U	3.5	8.3	0.04950	5.9	0.035	25.0
T45A60S	3DL	60	7,000	S	2	8.1	0.04950	5.8	0.035	14.3
T46A60S	3DL	60	7,000	S	3.2	8.1	0.04950	5.8	0.035	22.8
T47A60U	3DL	60	50,000	U	2.5	4.4	0.04950	3.1	0.035	17.8
T48A60U	3DC	60	3,000	U	2.5	4.4	0.03500	4.4	0.035	17.8
T49A45U	3DC	45	3,000	U	2	8.3	0.03500	8.3	0.035	14.3
T50A45U	3DC	45	3,000	U	1.5	8.3	0.03500	8.3	0.035	10.7
T51A30U	2DC	30	7,000	U	2.35	9.6	0.03500	9.6	0.035	16.8
T52A30U	2DC	30	50,000	U	3.2	9.6	0.03500	9.6	0.035	22.8
T53A30U	2DC	30	7,000	U	4.4	9.6	0.03500	9.6	0.035	31.4
T54A30S	2DC	30	4,000	S	4.4	10.3	0.03500	10.3	0.035	31.4
T55A30S	2DC	30	7,000	S	2.3	10.0	0.03500	10.0	0.035	16.4
T56A45S	2DC	45	7,000	S	2.3	10.3	0.03500	10.3	0.035	16.4
T57A45S	2DL	45	7,000	S	2.3	10.3	0.04950	7.3	0.035	16.4
T58A45S	2DL	45	4,000	S	4.1	10.3	0.04950	7.3	0.035	29.2

^aS=submerged; U=unsubmerged.

constant (Fig. 3). The upstream scour hole portion therefore only advances as z_m increases, whereas the ridge undergoes a substantial variation during this phase. At $t=125$ s, the scour hole base is cup shaped, because of the too steep tailwater scour hole portion. During this phase, its length from the maximum scour depth to the maximum ridge elevation (l_M-l_m) is made of two parts,

namely: (1) the active portion close to the maximum scour depth due to jet impact; and (2) the passive scour hole portion downstream, whose angle is essentially equal to ϕ . At $t=298$ s, the cup-shaped scour hole base is still visible, together with an intense sediment transport, pointing at the 3D scour hole expansion. At $t=1,200$ s, the ridge has reached its final shape, but the entire

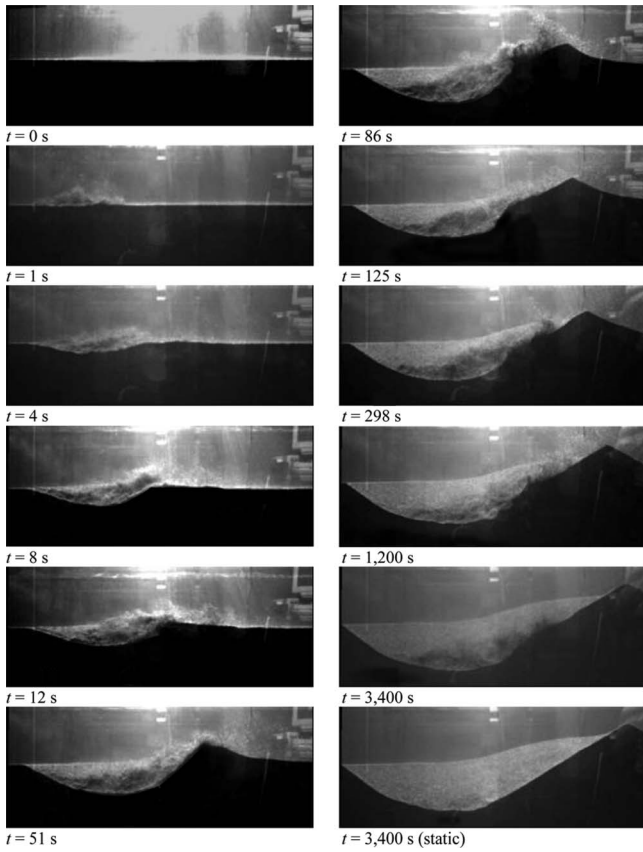


Fig. 3. Test T8A30S with $F_{d90}=33$, $\alpha=30^\circ$, S-jet, sequence of photos from $t=0$ to 3,400 s

formation still moves in the tailwater direction, as may be observed at $t=3,400$ s. The last photo relates to the static scour hole condition, i.e., after the jet flow was stopped. A notable difference occurs mainly at the scour hole base, where the “cup” portion has disappeared and the scour hole surface has slopes always equal to or smaller than ϕ .

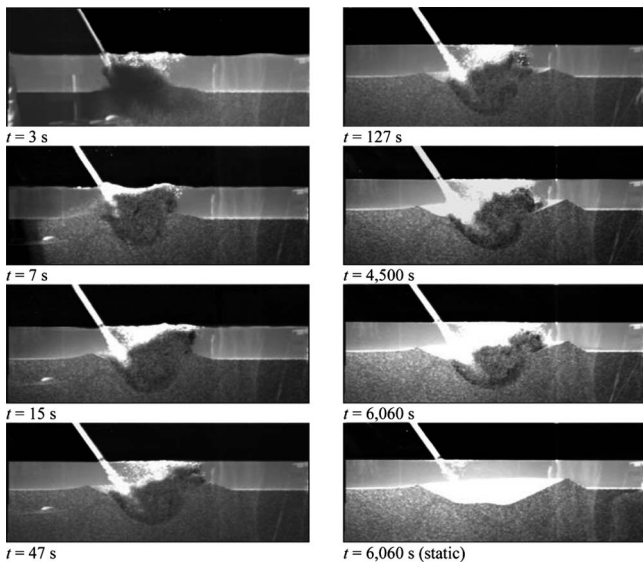


Fig. 4. Test T31A60U with $F_{d90}=27.8$, $\alpha=60^\circ$, U-jet, sequence of photos from $t=0$ to 6,060 s

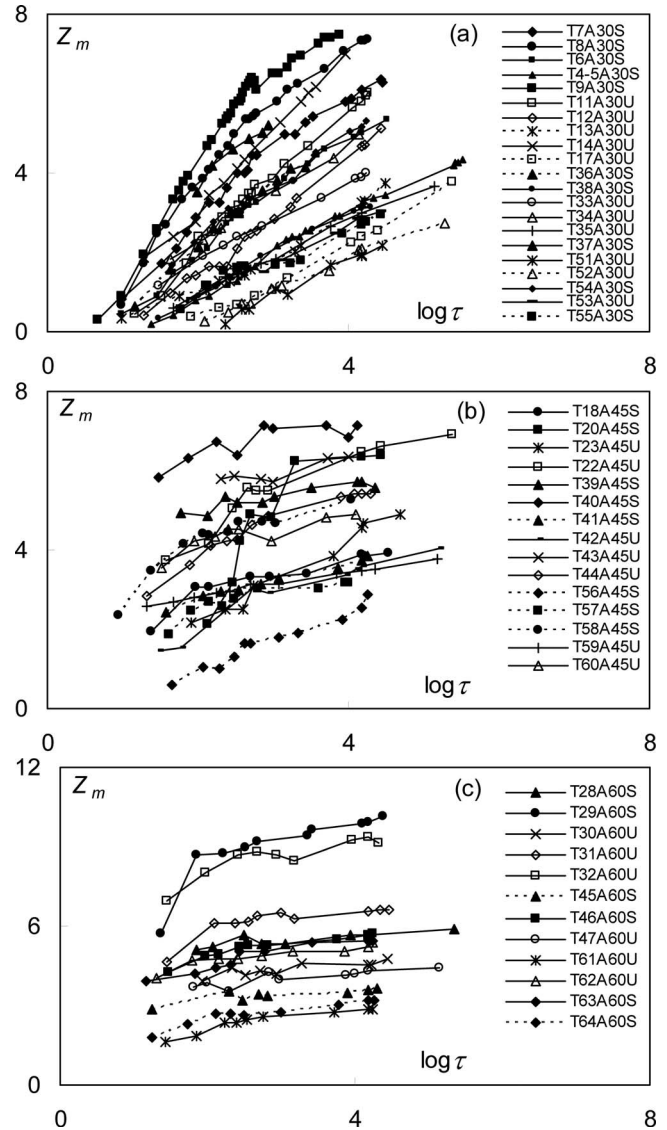


Fig. 5. Dimensionless scour hole depth $Z_m(\log \tau)$ for: $\alpha=(a)$ 30° ; (b) 45° ; and (c) 60° (light symbols=U-jets, full symbols=S-jets)

Fig. 4 relates to test T31A60U with $F_{d90}=27.8$, $\alpha=60^\circ$, and unsubmerged jet conditions, i.e., with a similar value of F_{d90} as in Fig. 3 but a large jet impact angle α . At time $t=3$ s, a sediment cloud limits visual access to the scour hole, which eventually moves in the tailwater direction as time progresses. From $t=7$ s, ridges both upstream and downstream of the jet impact point evolve, with the upstream ridge still under development at $t=4,500$ s. The observational quality of the scour hole surface for $\alpha=60^\circ$ is degraded due to suspended sediment. Therefore, no test was conducted for vertical jet impact. The geometries of the dynamic and the static scour holes at time $t=6,060$ s are completely different given the cup-shaped and much deeper scour hole for the dynamic conditions. Pagliara et al. (2004) noted that the latter is the relevant scour hole geometry in hydraulic engineering, because the static scour hole has a significantly smaller depth due to the deposition of the previously suspended sediment into the scour hole once the jet stops.

The nondimensional scour hole depth $Z_m=z_m/D$ versus nondimensional time $\tau=(g'd_{90})^{1/2} \cdot t/D$ as proposed by Oliveto and Hager (2002) is plotted semilogarithmically in Fig. 5 for $\alpha=30$,

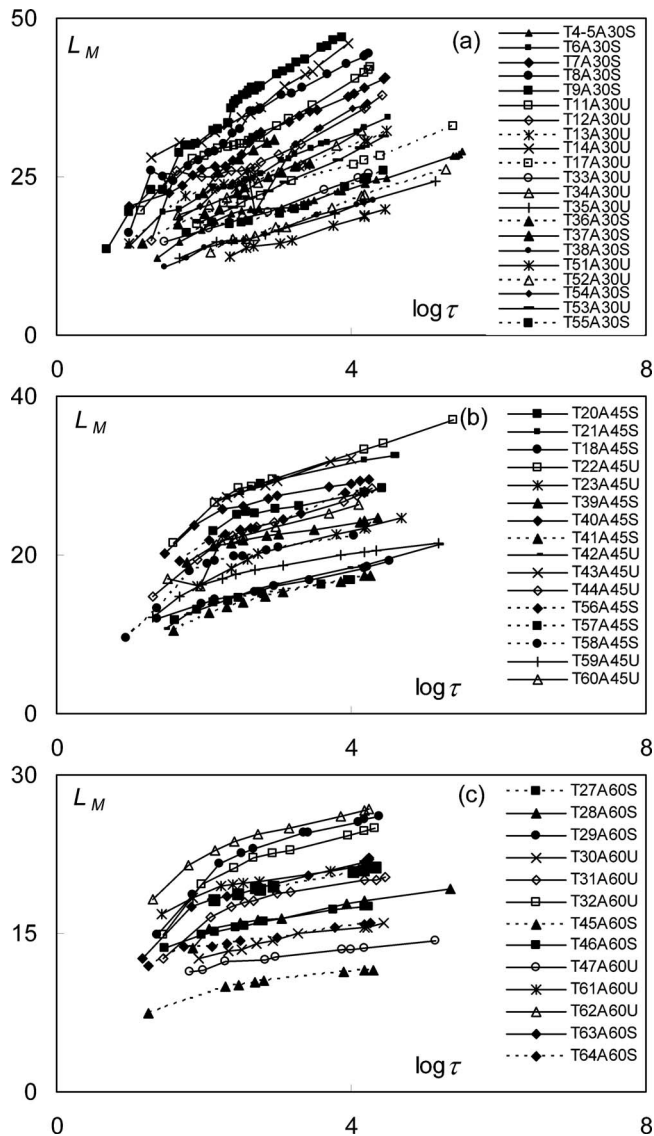


Fig. 6. Dimensionless location of maximum ridge height $L_M(\log \tau)$ for: α =(a) 30° ; (b) 45° ; and (c) 60° (light symbols=U-jets, full symbols=S-jets)

45, and 60 (see below). The slopes of these curves for a specific jet impact angle α remain nearly constant after a certain developing time for both S-jets or U-jets. Each straight may be defined with the slope and a virtual origin. A data analysis revealed that the developed scour hole regime may be defined at $\tau=15,000$ ($\log \tau=4.18$), corresponding to roughly $t=0.5$ h for the sediment and the jet diameters used. The “end scour” equations of Pagliara et al. (2006, 2008), listed in the Appendix, will be used below as a reference for describing the scour hole evolution. Similar plots as those for Z_m were also prepared for the dimensionless maximum ridge location $L_M=L_M/D$ versus $(\log \tau)$ in Fig. 6, and the dimensionless ridge height $Z_M=z_M/D$ versus $(\log \tau)$ in Fig. 7. Note that $Z < 0$ for elevations above the original sediment surface (Fig. 2).

Data Analysis

The temporal effect of two-phase flows following the Froude similitude depends on the densimetric particle Froude number

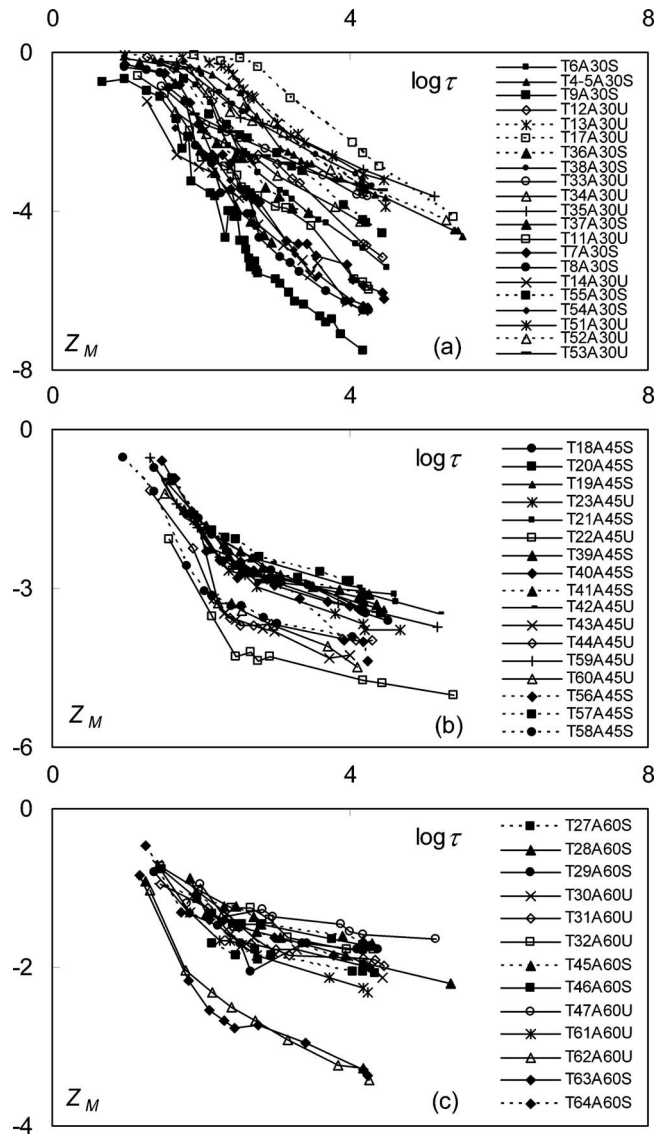


Fig. 7. Dimensionless ridge height $Z_M(\log \tau)$ for: α =(a) 30° ; (b) 45° ; and (c) 60° (light symbols=U-jets, full symbols=S-jets)

$F_d=V/V_R$ as the ratio of the effective to the reference (subscript R) velocities. With the reference length L_R such as the jet diameter D , and $V_R=(g'd)^{1/2}$ as the reference velocity, the temporal reference is $t_R=L_R/V_R$. For pier and plunge pool scour the pier and the jet diameters are the relevant reference lengths resulting in $t_R=D/(g'd)^{1/2}$. The relative time is $\tau=t/t_R=(g'd)^{1/2} \cdot t/D$, therefore, with $d=d_{90}$ (Pagliara et al. 2006).

Fig. 8 shows the reduced scour hole depth $\Delta Z_m=Z_m-Z_m(\tau=15,000)$ for $\alpha=30^\circ$ as a function of $(\log \tau)$ with $Z_m(\tau=15,000)$ from the Appendix. The data of the S-jets follow a slightly different trend than those of the U-jets. In both cases, the transition (subscript t) from the developing to the developed scour phase occurs in the range of $150 < \tau < 850$ ($2.2 < \log \tau < 3$). For $\tau > \tau_t$, the data follow $\Delta Z_m=-C_{1m}+C_{2m} \cdot \log \tau$, or $\Delta Z_m=C_{2m} \cdot \log(\tau/15,000)$. The parameter C_{2m} retains all effects of the “end scour,” whereas the temporal effect is reflected by the log term. The data for $\alpha=45$ and 60° were treated similarly. The terms C_{1m} and C_{2m} were plotted versus α for both the S- and the

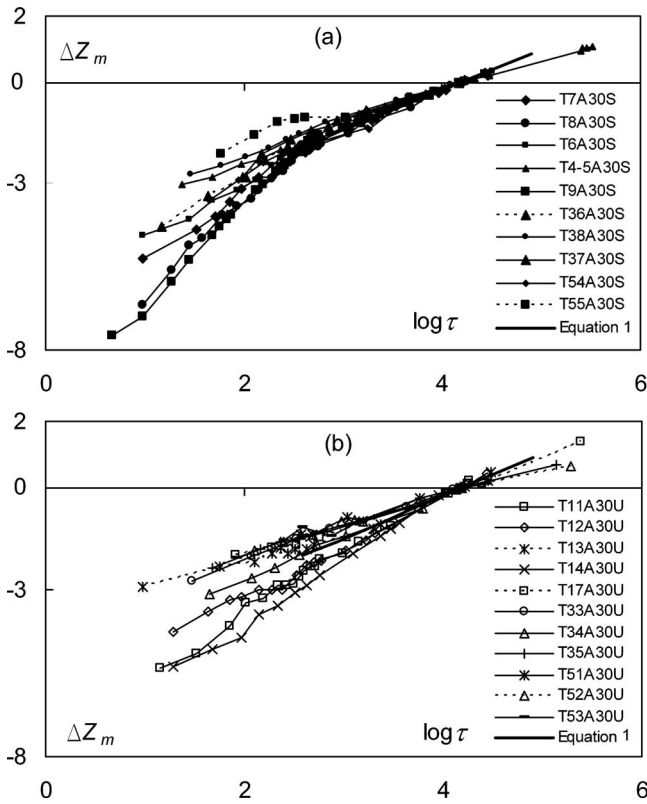


Fig. 8. Relative scour hole depth $\Delta Z_m(\log \tau)$ for $\alpha=30^\circ$ and: (a) S-jets; (b) U-jets

U-jets. The trend lines almost collapse and may be described with $A=1$ for S-jets and $A=1.12$ for U-jets with $\alpha(\text{deg})$ during the developed scour phase ($\tau > \tau_t$) as

$$\Delta Z_m = 2,000 \cdot A \cdot \alpha^{-2.2} \cdot \log(\tau/15,000) \quad (1)$$

Accordingly, unsubmerged jets produce a slightly larger scour hole depth, for otherwise identical flow conditions. To develop a final equation for $Z_m(\tau)$, the value $Z_m(\tau=15,000)$ from Eq. (15) in the Appendix plus the transition time τ_t must be known. The data indicated for $30^\circ \leq \alpha \leq 60^\circ$

$$\tau_t = A^2(-0.78\alpha^2 + 51.68\alpha - 150) \quad (2)$$

The parameter $Z_m(\tau=15,000)$ is plotted for the developed scour phase $\tau > \tau_t$ in Figs. 9 and 10 for $\alpha=30$ and 60° , respectively. The origin $(\log \tau; Z_m)=(0;0)$ was linearly connected with $Z_m(\tau=\tau_t)$ to describe the developing scour phase with $Z_{mi}=Z_m(\tau_t)$ as

$$Z_m/Z_{mi} = \log \tau / \log \tau_t, \quad \text{for } 0 < \tau < \tau_t \quad (3)$$

The equation for the developed scour phase is with τ_t from Eq. (2)

$$Z_m(\tau) = 2,000 \cdot A \cdot \alpha^{-2.2} \cdot \log(\tau/15,000) + Z_m(\tau = 15,000), \quad \text{for } \tau \geq \tau_t \quad (4)$$

Fig. 11(a) compares the test data with Eq. (3) for the developing, and Eq. (4) for the developed scour phases. The scatter about the line of perfect agreement is larger in the developing phase.

Other Parameters of Interest

The procedure was also applied to the location of the maximum ridge height $L_M(\tau)$, the maximum ridge elevation $Z_M(\tau)$, the locations of the maximum scour depth $L_m(\tau)$, and the scour hole

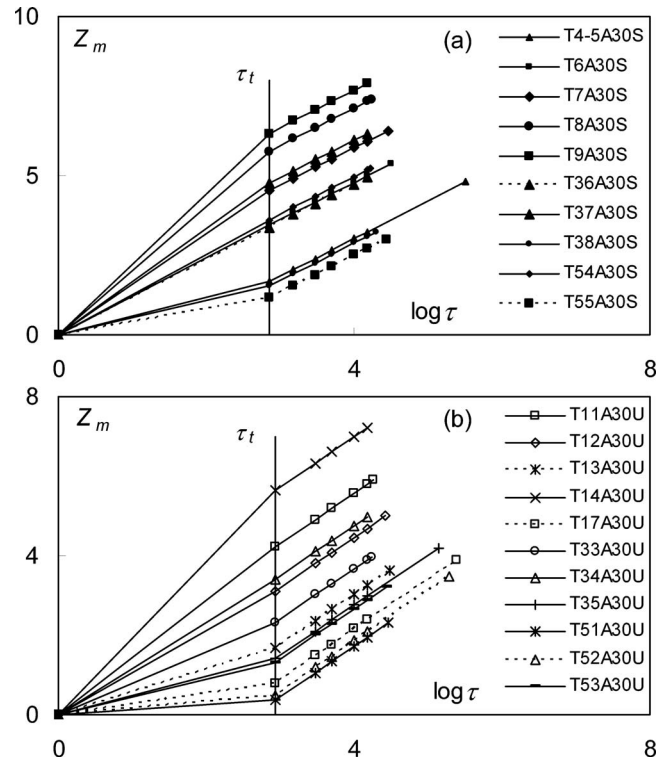


Fig. 9. $Z_m(\log \tau)$ for: $\alpha=30^\circ$ and (a) S-jets; (b) U-jets

intersection with the original bed level $L_d(\tau)$ (Fig. 2), to allow for a description of the entire scour hole geometry as a function of time, and the governing base parameters.

The location of the maximum ridge height $L_M=l_M/D$ was modeled as $Z_m(\tau)$ in Eqs. (3) and (4). The equation of the maxi-

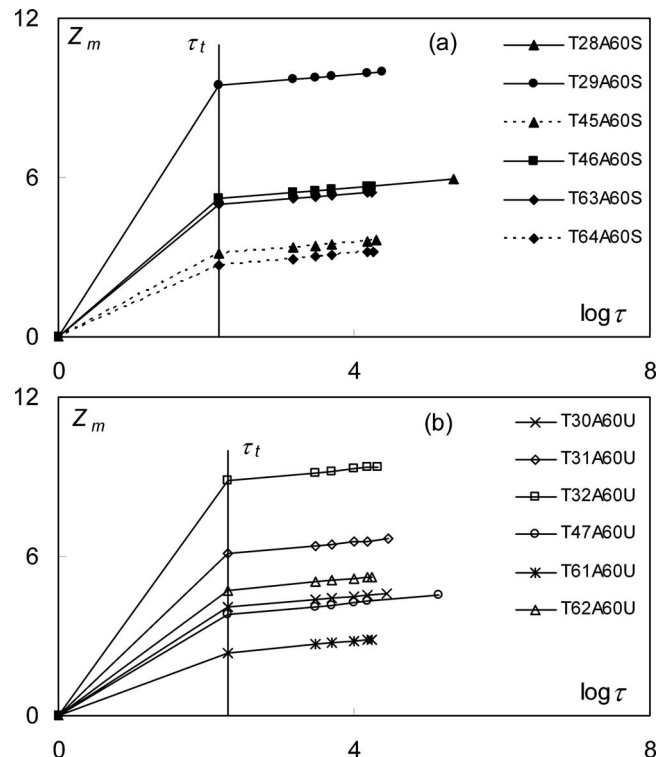


Fig. 10. $Z_m(\log \tau)$ for: $\alpha=60^\circ$ and (a) S-jets; (b) U-jets

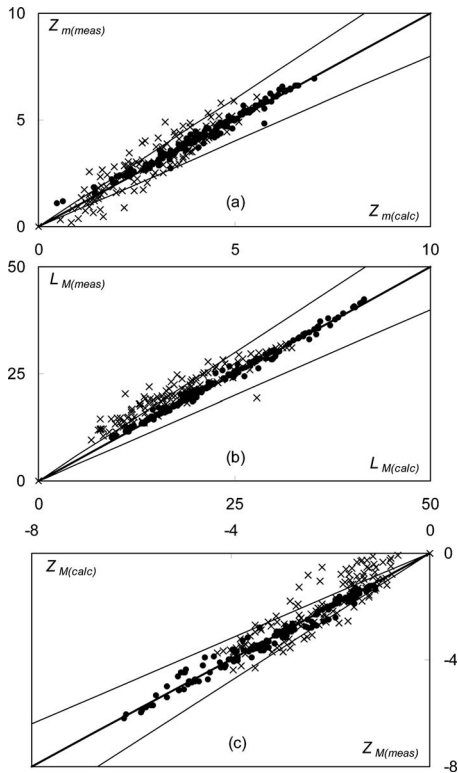


Fig. 11. Comparison between observations (meas) and predictions (calc) for (x) developing and (●) developed scour phases; (---) line of perfect agreement and (—) $\pm 20\%$ for evolution of: (a) maximum scour depth Z_m , $R^2=0.84$ (developing phase), $R^2=0.95$ (developed phase); (b) location of ridge L_M , $R^2=0.90$ (developing phase), $R^2=0.96$ (developed phase); and (c) ridge height Z_M with $R^2=0.78$ (developing phase), $R^2=0.95$ (developed phase)

imum ridge height location for $30^\circ \leq \alpha \leq 60^\circ$ reads with $L_M(\tau = 15,000)$ from Eq. (20) with $\mu_M=1.5$ for U-jets and $\mu_M=1$ for S-jets ($R^2=0.98$) during the developing scour phase

$$L_M/L_{Mt} = \log \tau / \log \tau_t, \quad \text{for } 0 < \tau < \tau_t \quad (5)$$

whereas the corresponding equation for the developed scour phase reads with $L_{Mt}=L_M(\tau_t)$

$$L_M = 8,800 \cdot A \alpha^{-2.2} \log(\tau/15,000) + L_M(\tau = 15,000), \quad \text{for } \tau \geq \tau_t \quad (6)$$

Eqs. (5) and (6) are compared with the test data in Fig. 11(b), involving a smaller scatter as the data for Z_m .

Fig. 12 relates to the quantity ΔZ_M versus $(\log \tau)$ of the maximum ridge elevation and the three jet impact angles investigated for U-jets. The data again collapse fairly well in the developed scour phase, whereas the data scatter is larger in the developing scour phase. With $R^2=0.98$, one has

$$\Delta Z_M = -C_{2M} \log \tau + C_{1M} = -2,300 \cdot (1/A) \cdot \alpha^{-2.2} \cdot \log(\tau/15,000) \quad (7)$$

The function Z_M versus $(\log \tau)$ in the developing scour phase was also assumed to increase linearly from $Z_M(\tau=0)$ to $Z_M(\tau_t)$, with τ_t from Eq. (2). The evolution of the maximum ridge height $Z_M(\tau)$ is

$$Z_M/Z_{Mt} = \log \tau / \log \tau_t, \quad \text{for } 0 < \tau < \tau_t \quad (8)$$

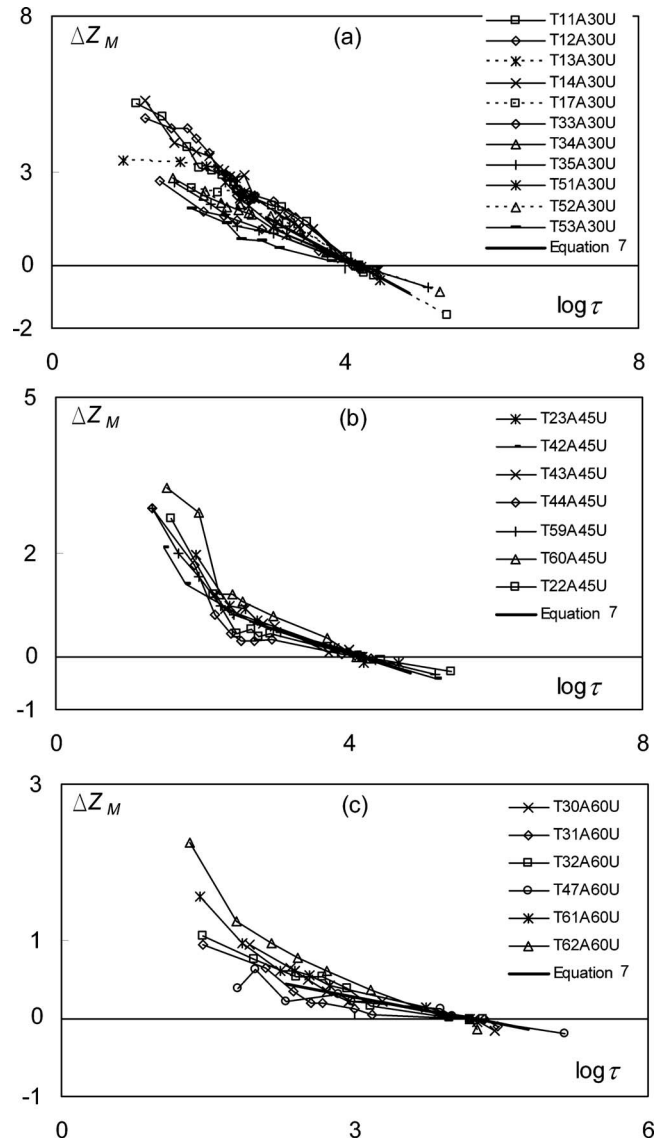


Fig. 12. $\Delta Z_M(\log \tau)$ for U-jets and $\alpha=(a) 30^\circ$; (b) 45° ; and (c) 60°

$$Z_M = 2,300 \cdot (1/A) \cdot \alpha^{-2.2} \cdot \log(\tau/15,000) - Z_M(\tau = 15,000), \quad \text{for } \tau \geq \tau_t \quad (9)$$

From Fig. 11(c) the test data compare reasonably well with Eqs. (8) and (9).

The locations of the dimensionless maximum scour depth $L_m=l_m/D$ and of the scour profile intersection with the original bed $L_a=l_a/D$ (Fig. 2) were also investigated. Fig. 13 relates to $\Delta L_a=L_a(\tau)-L_a(\tau=15,000)$ versus $(\log \tau)$, with $L_a(\tau=15,000)$ from Eq. (19). Because the differences between the S-jet and the U-jet data were small, only one relation was retained as ($R^2=0.99$)

$$L_a/L_{at} = \log \tau / \log \tau_t, \quad \text{for } 0 < \tau < \tau_t \quad (10)$$

$$L_a = 5,600 \cdot \alpha^{-2.2} \cdot \log(\tau/15,000) + L_a(\tau = 15,000), \quad \text{for } \tau \geq \tau_t \quad (11)$$

Following the previous procedure with $L_a(\tau=15,000)$ from Eq. (19) results for $30^\circ < \alpha < 60^\circ$ in

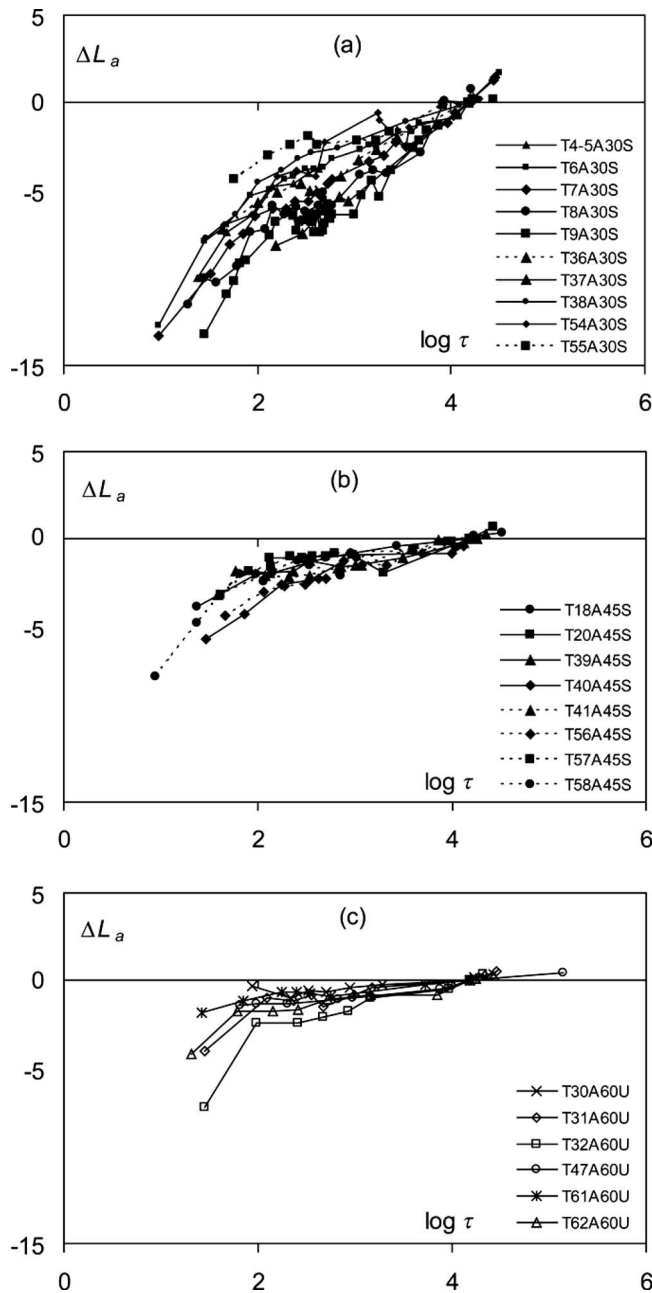


Fig. 13. Relative location of scour hole intersection with original bed level $\Delta L_a(\log \tau)$ for: (a) $\alpha=30^\circ$ and S-jets; (b) $\alpha=45^\circ$ and S-jets; and (c) $\alpha=60^\circ$ and U-jets

$$L_{at} = 5,600 \cdot \alpha^{-2.2} \cdot \log(\tau_t/15,000) + L_a(\tau = 15,000) \quad (12)$$

Fig. 14 shows excellent agreement of the test data with Eq. (12) for the developed and reasonable agreement with Eq. (11) for the developing scour phase.

Finally, the location L_m of the maximum scour hole depth was considered. With $L_m(\tau=15,000)$ from Eq. (18), the relations L_m versus $(\log \tau)$ for the two scour phases are

$$L_m/L_{mt} = \log \tau / \log \tau_t, \quad \text{for } 0 < \tau < \tau_t \quad (13)$$

$$L_m = (1.39 - 0.017\alpha)[\log \tau - 4] + L_m(\tau = 15,000), \quad \text{for } \tau > \tau_t \quad (14)$$

Fig. 14 shows essential agreement of the test data with Eq. (14) for the developed scour phase, whereas the scatter about the line

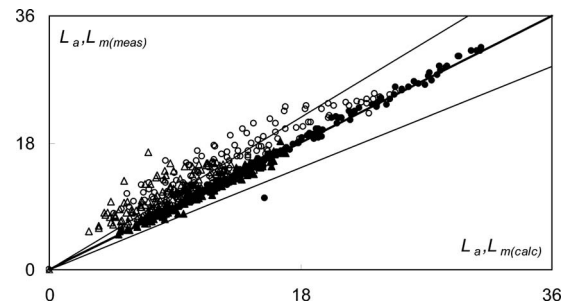


Fig. 14. Comparison between observations and predictions from Eqs. (10) and (13) for (○) L_a and (△) L_m during developing scour phase and from Eqs. (11) and (14) for (●) L_a and (▲) L_m during developed scour phase; (—) line of perfect agreement, (---) $\pm 20\%$ for temporal development of L_a , with $R^2=0.87$ (developing phase), $R^2=0.96$ (developed phase), location of scour maximum L_m , with $R^2=0.71$ (developing phase), $R^2=0.95$ (developed phase)

of perfect agreement is again larger in the developing scour phase. The origin of the scour hole profile $L_t(\tau=15,000)=l_t(\tau=15,000)/D$ as the distance to the jet impact point P (Fig. 2) was previously determined by Pagliara et al. (2008), as given in Eq. (17). The range of validity of this equation is as the relationship proposed in the Appendix.

Conclusions

The present research was conducted to analyze the temporal advance of plunge pool scour for a noncohesive sediment subjected to a circular jet under impact angles between 30 and 60° . Based on earlier work, in which the effects of the basic hydraulic parameters were investigated, and a time scale derived from the Froude similitude, the evolution of the major quantities describing the scour hole and the ridge geometry was analyzed. These quantities include the maximum scour hole depth and the ridge height, plus their locations relative to the scour hole origin. A novel test arrangement was designed to retain instantaneous scour hole profiles. This optical method could not be applied either to almost vertical jets or to cohesive material, because optical access was not assured.

A distinction was made between submerged and unsubmerged jets. The latter result in (slightly) larger scour, as expressed with the coefficient A . The effect of the jet impact angle is almost inversely quadratic, i.e., smaller angles produce a deeper and longer scour hole as do larger jet impact angles. The data analysis led to a distinction between the developing and the developed scour phases, separated at the transition time τ_t according to Eq. (2). The quantities investigated advance during both phases logarithmically with time, having a better agreement with the fitted equations during the developed than during the developing scour phase. Because all relations were derived from the test data, they are limited to the test conditions. The present research may be considered a first step toward the understanding of a highly complex and relevant process of scour hydraulics, which needs to be expanded to other fields of two-phase flows.

Appendix. Equation for Scour Depth at $\tau=15,000$

Pagliara et al. (2008) proposed the following relationship for the maximum practical “end scour depth”;

$$Z_m(\tau = 15,000) = -F_{d90} \cdot [0.38 \sin(\alpha + 22.5^\circ)] \cdot [(1 + \beta)^{-0.75}] \cdot (1/0.30)[0.12 \cdot \ln(1/T) + 0.45] \cdot [0.57\sigma + 0.33] \cdot [1.360 - 0.012\alpha^\circ] \cdot [4 + T] \cdot f(\lambda) \quad (15)$$

with the scour hole width function $f(\lambda)=0.140$ for $\lambda \leq 1.50$, and $[0.57\sigma+0.33] \cdot [1.360-0.012\alpha^\circ] f(\lambda)=1$ if $\lambda > 3.0$. Here $\lambda = B_m/B$ =relative scour hole width with B as the channel width and B_m =scour hole width. Eq. (15) applies for both plane and spatial scour holes, therefore. In the intermediate range $1.5 \leq \lambda \leq 3$ the effect of λ is linear between the two cases $\lambda=1.5$ and Eq. (15) is subject to the limitations: (1) $0.8 \leq T \leq 10$; (2) $30^\circ \leq \alpha \leq 60^\circ$; (3) $1 \leq F_{d90} \leq 30$; and (4) $\lambda \geq 0.20$.

The relative ridge height $Z_M = z_M/D$ at time $\tau=15,000$ is with α (deg) (Pagliara et al. 2008)

$$Z_M(\tau = 15,000) = ([0.010 + (0.044 - 0.001\alpha^\circ) \cdot T] \cdot F_{d90} + 0.800) \cdot (0.815 + 0.507\lambda) \quad (16)$$

subject to the same limitations as above.

The length characteristics of the scour hole profile may be described with the parameters $L_i = l_i/D$, $L_m = l_m/D$, $L_a = l_a/D$, and $L_M = l_M/D$ (Fig. 2). Pagliara et al.'s (2006, 2008) expressions at $\tau=15,000$ are

$$L_i = [(0.035 + 0.034T - 0.001\alpha^\circ) \cdot F_{d90} + (7.667 - 0.100\alpha^\circ)] \cdot (1.285 - 0.361\lambda) \quad (17)$$

$$L_m = [1.5 + (1 - 0.01\alpha^\circ)F_{d90}] \cdot \zeta_{LmT} \quad (18)$$

$$L_a = 2.5[1 + 1.05 \cdot \exp(-0.030\alpha^\circ) \cdot F_{d90}] \cdot \zeta_{LaT} \quad (19)$$

$$L_M = 2.5[1 + 30\mu_M\alpha^{-1.25}F_{d90}], \quad (20)$$

with

$$\zeta_{LmT} = [1.705 - 0.012\alpha^\circ - 0.010F_{d90}] \cdot [0.719 + 0.061T] \quad \text{for } \lambda < 1.50 \quad (21)$$

$$\zeta_{LaT} = [0.168 + 0.062T + 0.020\alpha^\circ] \cdot [1.217 - 0.013F_{d90}] \cdot [0.851 + 0.345\lambda] \quad \text{for } \lambda \leq 1.50 \quad (22)$$

and $\zeta_{LmT} = \zeta_{LaT} = 1$ for $\lambda > 3$. Apply a linear interpolation between the limits $\lambda=1.50$ and $\lambda=3$.

Notation

The following symbols are used in this paper:

- A = factor of proportionality, $A=1$ for S-jets, $A=1.12$ for U-jets;
- B = channel width;
- B_m = scour hole width;
- C = constant;
- D = jet diameter;
- d = sediment diameter;
- F_d = $V/(g'd)^{1/2}$ densimetric Froude number;
- g = gravitational acceleration;
- g' = $[(\rho_s - \rho)/\rho]g$ reduced gravitational acceleration;
- h = free surface elevation;
- L = l/D relative length;
- l = length from origin;

- Q = discharge;
- R^2 = correlation coefficient;
- T = h_o/D relative tailwater elevation;
- t = time;
- V = average jet velocity;
- x = streamwise coordinate;
- Z = z/D relative depth or height;
- z = vertical coordinate;
- α = jet impact angle;
- β = jet air content;
- λ = B_m/B relative scour width;
- μ = effect of jet regime;
- ρ = density;
- σ = $(d_{84}/d_{16})^{1/2}$ sediment nonuniformity;
- τ = $(g'd_{90})^{1/2} \cdot t/D$ dimensionless time; and
- ϕ = sediment angle of repose.

Subscripts

- a = scour hole end;
- L = relative to length L ;
- M = maximum ridge elevation;
- m = maximum scour depth;
- R = reference;
- s = sediment;
- t = transition;
- test = experimental test; and
- u = ridge end.

References

- Anderson, C. L., and Blaisdell, F. W. (1982). "Plunge pool energy dissipators for pipe spillways." *Proc., Conf. Applying Research to Hydraulic Practice*, P. E. Smith, ed., ASCE, New York, 289–298.
- Bormann, N. E., and Julien, P. Y. (1991). "Scour downstream of grade-control structures." *J. Hydraul. Eng.*, 117(5), 579–594.
- Canepa, S., and Hager, W. H. (2003). "Effect of air jet content on plunge pool scour." *J. Hydraul. Eng.*, 128(5), 358–365.
- Chiew, Y.-M., and Lim, S.-Y. (1996). "Local scour by a deeply submerged horizontal circular jet." *J. Hydraul. Eng.*, 122(9), 529–532.
- Dey, S., and Barbhuiya, A. K. (2005). "Time variation of scour at abutments." *J. Hydraul. Eng.*, 131(1), 11–23.
- Hager, W. H., Unger, J., and Oliveto, G. (2002). "Entrainment criterion for bridge piers and abutments." *River flow 2002*, D. Bousmar and Y. Zech, eds., Swets & Zeitlinger, Lisse, The Netherlands, 1053–1058.
- Oliveto, G., and Hager, W. H. (2002). "Temporal evolution of clear-water pier and abutment scour." *J. Hydraul. Eng.*, 128(9), 811–820.
- Pagliara, S., Amidei, M., and Hager, W. H. (2008). "Hydraulics of 3D plunge pool scour." *J. Hydraul. Eng.*, 134(9), 1275–1284.
- Pagliara, S., Hager, W. H., and Minor, H.-E. (2004). "Plunge pool scour in prototype and laboratory." *Proc., Int. Conf. Hydraulics of Dams and River Structures*, Balkema, Lisse, The Netherlands, 165–172.
- Pagliara, S., Hager, W. H., and Minor, H.-E. (2006). "Hydraulics of plane plunge pool scour." *J. Hydraul. Eng.*, 132(5), 450–461.
- Rajaratnam, N. (1980). "Erosion by circular wall jets in cross flow." *J. Hydr. Div.*, 106(11), 1867–1883.
- Rajaratnam, N., and Berry, B. (1977). "Erosion by circular turbulent wall jets." *J. Hydraul. Res.*, 15(3), 277–289.
- Unger, J. (2006). "Strömungscharakteristika um kreiszylindrische Brückenpfeiler—Anwendung von Particle Image Velocimetry in der Kolkhydraulik." Ph.D. thesis, Switzerland, ETH, Zurich (in German).
- Unger, J., and Hager, W. H. (2007). "Down-flow and horseshoe vortex characteristics of sediment embedded bridge piers." *Exp. Fluids*, 42(1), 1–19.